Voltage Dynamics of Current Control Time-Scale in a VSC-Connected Weak Grid

Mingquan Zhao, *Student Member, IEEE*, Xiaoming Yuan, *Senior Member, IEEE*, Jiabing Hu, *Senior Member, IEEE*, and Yabing Yan, *Student Member, IEEE*

***Abstract*—Voltage problems are challenging in modern power systems with a high penetration of renewables integrated via power electronics. This paper extends the transient time-scale classification to identify voltage dynamics in modern power systems. Voltage dynamics in the current control time-scale is firstly proposed and then the mechanism of terminal voltage change is elaborated. After that the significant influences of the voltage source converter (VSC), current control (CC) loop and voltage feed forward (VFF) on the voltage dynamics in the current control time-scale are discussed. The VSC current control loop provides positive damping on the terminal voltage, while the VFF scheme results in an additional loop that deteriorates terminal voltage dynamic performance and stability. In addition, a sensitivity analysis was carried out to investigate the influence of critical parameters on stability. Finally, simulation results of a current-controlled VSC attached to different strength of AC grids (including a weak grid) are presented to validate the phenomenon and the influencing factors of voltage dynamics in the current control time-scale.**

***Index Terms*—Current control, voltage dynamics, voltage feed forward (VFF), voltage source converter (VSC), weak grid, wind turbine generator (WTG).**

NOMENCLATURE

T_s	Sample time of converter
T_{PWM}	Time constant of the PWM block
ω_0	Resonant frequency of the P-Resonant control
α_f	Bandwidth of VFF low-pass filter (rad/s)
C	LC-filter capacitance
L_1	LC-filter inductance
L_2, R_2	Transmission line inductance and reactance
u_1	Converter voltage
u_2	Grid voltage
u_t	Terminal voltage

Superscript:

*	Signals reference

Subscripts:

dq	Rotating reference frame signal direct-axis and quadrature-axis components
t	Terminal signals of VSC
$1, 2$	Converter and grid signals
C	Signals on LC-filter capacitor

Manuscript received February 05, 2015; revised May 05, 2015, July 12, 2015, and September 09, 2015; accepted September 12, 2015. Date of publication October 05, 2015; date of current version May 02, 2016. This work was supported in part by National Basic Research Program of China (973 Program) under Grant 2012CB215100, in part by the Major Program of National Natural Science Foundation of China under Grant 51190104, in part by the Science and Technology Program of State Grid Corporation of China under Grant 2013320001510213 and XT71-14-051, and in part by the National Natural Science Fund for Excellent Young Scholars under Grant 51322704. Paper no. TPWRS-00162-2015.

The authors are with State Key Laboratory of Advanced Electromagnetic Engineering and Technology, and School of Electrical and Electronic Engineering, Huazhong University of Science and Technology, Wuhan 430074, China (e-mail: zhaomq@hust.edu.cn; yuanxm@hust.edu.cn; j.hu@hust.edu.cn; YB_Yan@hust.edu.cn).

Color versions of one or more of the figures in this paper are available online at http://ieeexplore.ieee.org.

Digital Object Identifier 10.1109/TPWRS.2015.2482605

I. INTRODUCTION

IN modern electrical grids, more and more wind power generators and photovoltaic inverters have become attached to weak grids since the renewable energy resources are usually located far from load centers. As a result, large-scale generating facilities connected to weak grids bring many new challenges to system operation and security [1], [2]. Some actual voltage-unstable phenomena have already been captured in real-time wind power plant operations [3]. Consequently, the voltage dynamics issue of high wind generation penetration in weak grids has received increasing attentions from independent system operators (ISOs) and researchers.

The voltage dynamics analysis is always divided into two perspectives of amplitude and phase, which are classified as voltage stability and angle stability problem. However, this paper analyzes voltage dynamics as a whole, neither from voltage stability nor angle stability alone. Actually, the rational analysis depends on the accurate classification of time-scales. In conventional power system, the problem of voltage stability is divided into several different time-scales in a qualitative way [4]–[8]. For long-term time-scale, researchers have focused on static voltage stability, while for mid-time-scale some slow control dynamics have been considered. A lot of work has been done in these time-scales, with some valuable conclusions provided in [9]–[11]. However, the problem of dynamic voltage stability in transient time-scale has not been fully researched. This problem becomes more complicated when an increasing number of power electronics are connected to a grid. The control loops in power electronics are generally faster than those in the synchronous generator (SG). As an example, current control, faster than any control loops in the SG, is very often contained within power electronics. Therefore, traditional time-scale classification method

for voltage stability can make analysis confusing and in fact may not be applicable in some cases. In this paper, an extended time-scale classification method appropriate for power systems with highly-penetrated power electronics is presented that explicitly adjusts according to the different response speeds of the various control loops.

It is worth noting that, the stability issues caused by renewable energy generations connected to weak grids are completely different from the characteristics of such systems in stiff grids. In the past, lots of researches were carried out only from maintaining the stability of equipment output, which did not sufficiently concern the stability of other equipment in the power systems. It is reasonable since that the analyses are always based on the stiff grids condition. However, for weak grids, it is not applicable to identify a stable terminal voltage, as has been generally assumed in the past. When power electronic equipment is integrated into a weak grid, the terminal voltage is more sensitive to the dynamics of the equipment's output than the terminal voltage in stiff grids [12]. So the analyses in this paper are especially carried out to investigate the effects of power electronic equipment on the state of power systems. Recently, more and more researchers have become aware of the voltage problems that can occur when voltage source converters (VSCs) are connected to weak grids. The voltage control challenges and voltage stability issues in weak grids have been shown in [1]–[3]. Some preliminary researches efforts have studied voltage dynamics in the terminal voltage control time-scale [13]–[17], but little work has been done in the current control time-scale, which is much faster. This paper focuses on voltage dynamics in current control time-scale.

Among the existing control strategies for power electronics, voltage feed forward (VFF) is a popular scheme that belongs to the current control loop family of controllers [18]. A well-known potential use for VFF is in improving the output current dynamics of a grid suffering a disturbance. Some work has been done towards developing VFF techniques through two aspects: improving self-stability and dynamics [19]–[21] and affecting system electrical damping [22]. In [19], a voltage feed-forward part with a proportional factor was added to improve response speed to a voltage disturbance, while [20] proposed a novel control to actively damp resonance in the input LC filter that used a lead–lag element in the VFF to effectively damp oscillations of the VSC. In [21], a feed-forward grid voltage disturbance rejection scheme was proposed as a means of further reducing the level of low-order current harmonic distortion. In [22], Lennart Harnefors analyzed the effect of point of common coupling (PCC)-voltage feed-forward on system electrical damping, proving that increasing the low-pass filter bandwidth of the PCC-voltage feed-forward enlarges the region where negative resistance and negative electrical damping are obtained for proportional-integral (PI) control with PCC-voltage feed-forward.

While VFF systems in general have received a lot of attention, as described above, the effect of VFF on terminal voltage dynamics has been totally neglected. When an ideal VFF is considered, the converter current does not respond to any grid disturbances, and the VSC contributes nothing to the voltage dynamics damping. In fact, if there are no devices providing damping for a grid disturbance, the system becomes unstable. So the design of equipment controller should consider the influence on the other equipment stability. As such, this paper focuses on the change mechanism of the terminal voltage and analyzes the effect of VFF from the perspective of voltage damping.

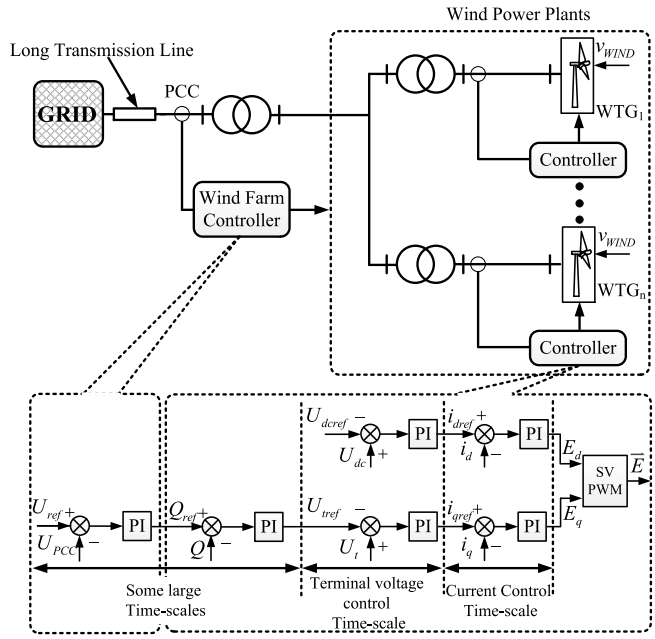

Fig. 1. Simplified diagram of WPP integrates into power grid (Type4).

The rest part of this paper is organized as follows. Section II proposes an extended time-scales decomposition method and briefly illustrates the studied system and the model equivalence is briefly illustrated. Section III focuses on the mechanisms behind changes in the terminal voltage, and proposes the small signal modelling for terminal voltage dynamics stability analysis of a VSC system. In Section IV, the effects of current control, VFF and AC grid strength on terminal voltage dynamics stability and the sensitivity of critical parameters are fully investigated. Simulation studies for validating the above analyses are carried out in Section V. Section VI discusses some related issues concerning terminal voltage, while Section VII briefly draws several conclusions.

II. Voltage Dynamics Analysis Time-Scales Decomposition Method and Analysis Model

A. Time-Scales Decomposition Method

When analyzing power system stability, the time frame of the concerned problem may vary from a few milliseconds to tens of minutes. These time-scales are usually decomposed according to the statuses of the different equipment components or the response speeds of the different control loops after a disturbance. Actually, these time-scales have been already identified in conventional power systems in a qualitative way. However, power electronics equipment have been increasingly utilized in modern power systems. With these systems, faster control loops such as current control loops have been proposed to control power electronics equipment for different control objectives. Thus, the conventional decomposition method [4]–[8] is coarse

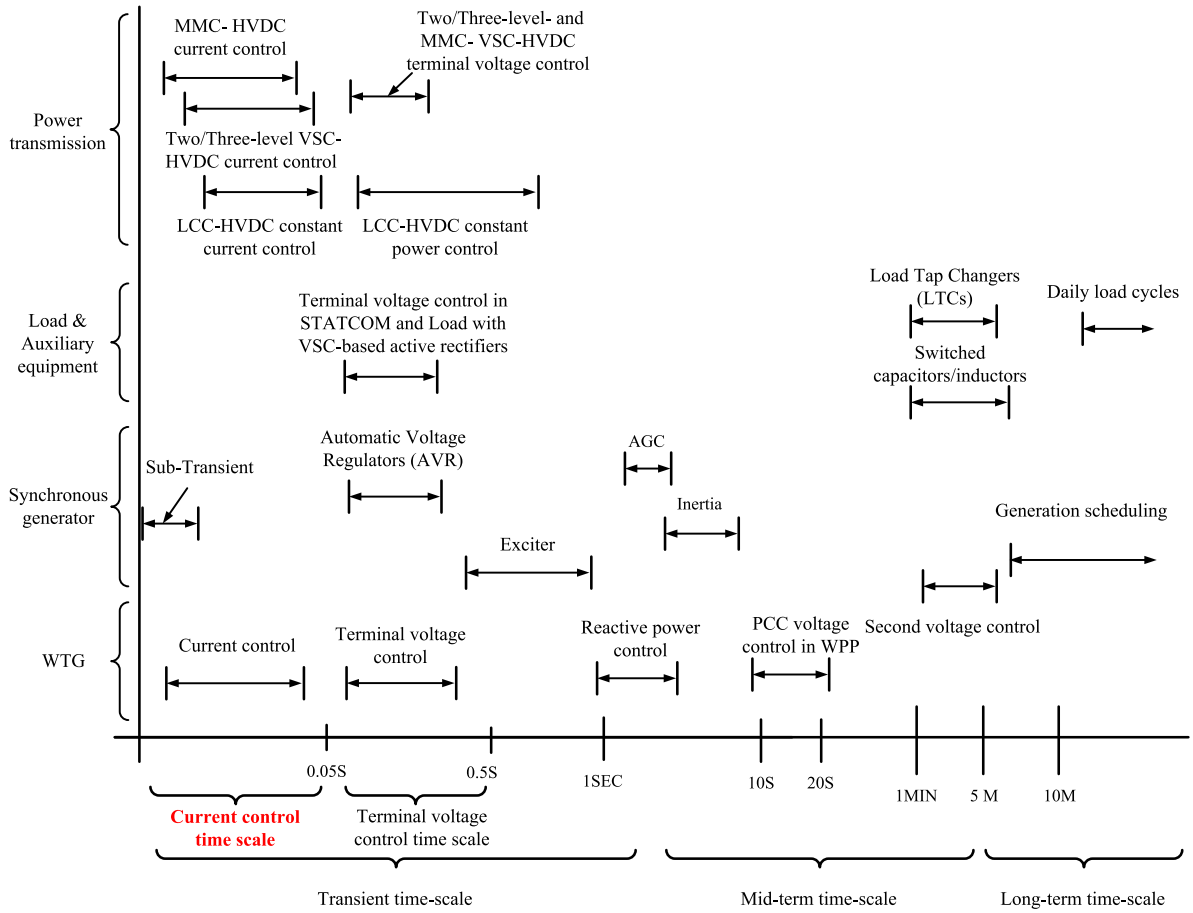

Fig. 2. The extended time-scale decomposition method for voltage dynamics analysis and the representative time constants of critical facilities.

for simplification and order reduction of complex systems when analyzing dynamic voltage stability problems, and the analysis of voltage dynamics becomes very difficult for transient time-scale due to the confusion caused by incorrect time-scale classification. Therefore, it is necessary to refine the time-scales when dealing with voltage stability phenomena.

Taking the wind power plant (Type 4) shown in Fig. 1 as an example, current control, terminal voltage control, and reactive power control are included in the wind turbine generator (WTG) system. Moreover, the wind power plant (WPP) controller maintains voltage control over the PCCs in the system, and has a longer response time [23]. According to the different response times of the control loops, this paper classifies the transient time-scale of the voltage problem into a terminal voltage control time-scale (approximately 50 ms to 1 s) and a current control time-scale (less than 50 ms). The precise distinction between the two time-scales depends on the response time of the controller of each element. For a clearer illustration of this distinction, Fig. 2 depicts the extended voltage dynamics analysis time-scale classification that contains the additional power converter control time-scale.

Fig. 2 also displays some representative time constants in power systems for typical facilities, which can help in more intuitively understanding the extended time-scale classification.

In terminal voltage control time-scale, we must consider the quasi steady state representation of the power electronics equipment. The output current of this equipment can be considered equal to the current reference since the bandwidth of the terminal voltage control is set much smaller than the current control. On the other hand, the terminal voltage control loop does not respond within the time-scale of the current control, so all current references can be regarded as constant. However, all elements related to the current control loop must be fully considered, particularly the electromagnetic and network transients.

B. Modelling and Simplification of Studied System

1) Studied System and Control Strategy: Fig. 1 shows the WPP integrated into the power grid through a long transmission line. In general, a wind generation voltage control system includes two control levels providing WPP and WTG control. In recent years, we have seen WTG voltage stability problems frequently appearing not only in academic research but also in actual operation [2], [3], [13]–[17].

In order to analyze the voltage dynamics of only one machine, this paper studies voltage dynamics by examining the case of a VSC transporting electrical power to an infinite grid via a well-designed LC filter and grid impedance. The general system for investigation is shown in Fig. 3. This circuit can be regarded as the simplification of a multi-generator system. Thus, the external reactance X_2 and infinite bus $\boldsymbol{U}_2$ represent the grid as seen from the terminal of the machine studied. Analysis of a

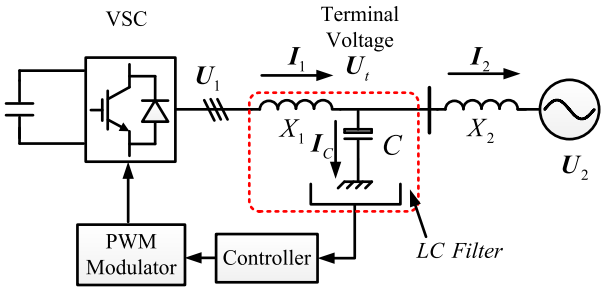

Fig. 3. Simplified diagram of studied system.

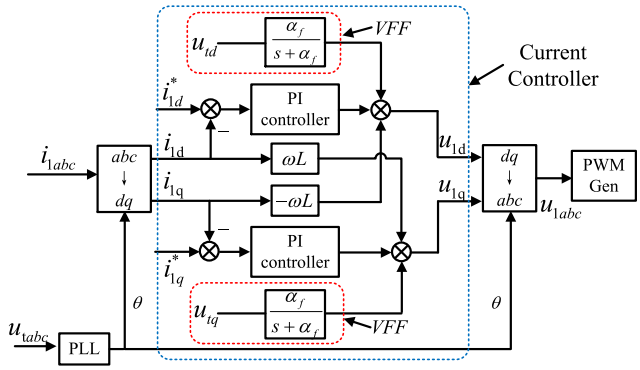

Fig. 4. Generic current control scheme of VSC.

system having such a simple configuration is extremely useful in understanding some basic concepts.

In Fig. 3, capacitor C provides a low-impedance path for the high frequency harmonic current, which decreases the harmonic component of the VSC output current $\boldsymbol{I}_1$. The voltage across the capacitor is generally regarded as the VSC terminal voltage.

To study voltage dynamics in the current control time-scale, several assumptions must be made:

- The DC bus voltage is constant and the three-phase system is balanced. Therefore, the VSC can generate any required current.
- The VSC's switching frequency is sufficiently high that it will have a negligible effect on VSC control.
- In the current control time-scale, slower outer loops such as the power control loop and the voltage control loop do not respond instantaneously when a disturbance occurs.

Using the above assumptions, the VSC can be represented as an "average switching model (ASM)" and the current references are all constants.

The details of the control system are illustrated in Fig. 4, which briefly describes the widely used current control scheme in a VSC [24]. For simplicity, Fig. 4 only retains the current control loop, while the outer loop is ignored. The cross-coupling terms and VFF signals are added to the outputs of the current regulators to improve the performance of the current control loop.

Proper design of a system's VFF is a typical method used to improve the dynamic performance of the output current while ignoring the stability of the terminal voltage. This approach is achieved by adding a measured VSC terminal voltage variation to the outputs of the current regulators, which always use a low-pass filter to improve their disturbance rejection capability. The resultant signals, which sum the outputs of each current regulator and its corresponding compensation term, are then transformed to the stationary *abc* reference frame as commands to the pulse width modulator (PWM) generator.

A proportional-resonant (P+Resonant or PR) controller is another possible way to structure the control loops, which is used in a stationary reference frame. Due to its advantages in operations under unbalanced conditions, PR controllers have gained some popularity for providing current regulation in grid-connected systems [18], [25], [26]. Moreover, the modeling of a VSC does not need to use the model equivalent method under this subsection, since the PR controller is already in the stationary reference frame. After some adjustments to the actual situation, the corresponding analysis method described in Section III can be used directly. However, this paper still takes the control system shown in Fig. 4 as the investigated object, because it is one of the most popular current regulation methods for VSC control.

2) The Model Equivalent Method: A synchronous frame PI (SRFPI) controller is widely used for converters. The generic implementation of a SRFPI control is depicted in Fig. 4, with the transfer function of a SRFPI controller in the synchronous frame is given by

$$\begin{bmatrix} u_{1d}^* \\ u_{1q}^* \end{bmatrix} = \underbrace{\begin{bmatrix} K_p + \frac{K_i}{s} & 0 \\ 0 & K_p + \frac{K_i}{s} \end{bmatrix}}_{G_c^{dq}(s)} \left\{ \begin{bmatrix} i_{1d}^* \\ i_{1q}^* \end{bmatrix} - \begin{bmatrix} i_{1d} \\ i_{1q} \end{bmatrix} \right\} \quad (1)$$

which neglects the VFF and current cross-coupling terms. Using the transformation techniques described in [26], the equivalent transfer function in the stationary *abc* frame can be derived as (2), shown at the bottom of the page. These significant off-diagonal terms represent cross coupling between phases. However, [27] confirmed that the cross-coupling terms of a SRFPI system only have a small influence around the fundamental frequency.

$$G_c^{abc}(s) = \frac{2}{3} \begin{bmatrix} K_p + \frac{K_i s}{s^2+\omega^2} & -\frac{1}{2}K_p + \frac{-\frac{1}{2K_i}s - \frac{\sqrt{3}}{2K_i}\omega}{s^2+\omega^2} & -\frac{1}{2}K_p + \frac{-\frac{1}{2K_i}s + \frac{\sqrt{3}}{2K_i}\omega}{s^2+\omega^2} \\ -\frac{1}{2}K_p + \frac{-\frac{1}{2K_i}s + \frac{\sqrt{3}}{2K_i}\omega}{s^2+\omega^2} & K_p + \frac{K_i s}{s^2+\omega^2} & -\frac{1}{2}K_p + \frac{-\frac{1}{2K_i}s - \frac{\sqrt{3}}{2K_i}\omega}{s^2+\omega^2} \\ -\frac{1}{2}K_p + \frac{-\frac{1}{2K_i}s - \frac{\sqrt{3}}{2K_i}\omega}{s^2+\omega^2} & -\frac{1}{2}K_p + \frac{-\frac{1}{2K_i}s + \frac{\sqrt{3}}{2K_i}\omega}{s^2+\omega^2} & K_p + \frac{K_i s}{s^2+\omega^2} \end{bmatrix} \quad (2)$$

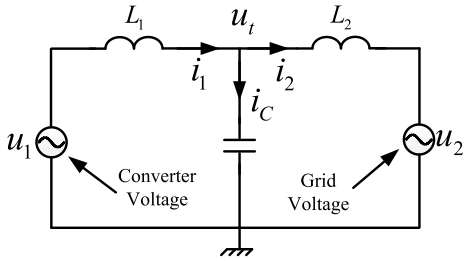

Fig. 5. Block diagram of stability analysis model.

Outside of this region, SRFPI and the PR controllers have practically identical performance characteristics. The PR controller can be described by

$$G_c(s) = K_p + \frac{K_i s}{s^2 + \omega_0^2} \tag{3}$$

where ω_0 is the resonant frequency of the integrator corresponding to the signal frequency. Note that the PR controller is already in the stationary *abc* frame and ensures that the phases are independent from one another.

Because of the characteristics mentioned above, a single-phase stability analysis of a PR scheme can be directly applied to determine the transient performance of a SRFPI controller in the current control time-scale. Consequently, this paper will substitute the PI controller in the *dq* rotating frame with a PR controller in the *abc* frame to analyze terminal voltage dynamics in the current control time-scale. This equivalence is quite useful for simplifying the problem.

3) System Modelling: It is well known through [20] that the delay time consists of the two smallest time constants, the sample delay (equal to T_s) and the PWM implementation delay (approximately equal to $0.5T_s$), i.e.,

$$T \approx T_s + T_{PWM} = 1.5T_s \tag{4}$$

where T represents the equivalent delay time that groups the sample delay and the PWM dead time together.

The digital signal processing and the delay introduced by the PWM converter occur in the stationary reference frame. The equivalent delay can be approximated by a first-order transfer function in the synchronous reference frame

$$G_d(s) = \frac{1}{1 + T(s + j\omega)} \approx \frac{1}{1 + Ts}. \tag{5}$$

The cross-coupling effects are introduced by the transformation filter when transforming from the synchronous reference frame to the stationary reference frame. Nonetheless, it is customary to neglect all signals that multiply by imaginary gain coefficients when designing the current controllers [28]. On the other hand, the VFF is essentially implemented in the synchronous reference frame, so for simplicity the transfer function of the VFF filter need to approximate

$$G_l(s) \approx \frac{\alpha_f}{s + \alpha_f}. \tag{6}$$

According to the model equivalent method described in the previous subsection, the PR controller used in this model, can be re-presented by $G_c(s)$, while $G_d(s)$ represents the transfer function of the delay part of the VSC. The converter voltage of the VSC control without VFF can be written as

$$u_{1k} = \underbrace{\left(K_p + \frac{K_i s}{s^2 + \omega_0^2}\right)}_{G_c(s)} \underbrace{\left(\frac{1}{1 + Ts}\right)}_{G_d(s)} (i_k^* - i_k), \quad k = a, b, c. \tag{7}$$

On the other hand, when VFF signals are added to the VSC control, the converter voltage is given as

$$u_{1k} = \left[\underbrace{\left(K_p + \frac{K_i s}{s^2 + \omega_0^2}\right)}_{G_c(s)} (i_k^* - i_k) + \underbrace{\left(\frac{\alpha_f}{s + \alpha_f}\right)}_{G_l(s)} u_{tk}\right] \cdot \underbrace{\left(\frac{1}{1 + Ts}\right)}_{G_d(s)}, \quad k = a, b, c \tag{8}$$

where $G_l(s)$ is the transfer function of the VFF low-pass filter, which has a bandwidth α_f.

For a three-phase symmetric system, the following set of equations describes the voltage and current conditions on the LC filter and the grid impedance

$$\begin{aligned} L_1 \frac{di_{1k}}{dt} &= u_{1k} - u_{tk} - i_{1k} R_1 \\ C \frac{du_{tk}}{dt} &= i_{Ck} \\ L_2 \frac{di_{2k}}{dt} &= u_{tk} - u_{2k} - i_{2k} R_2 \quad k = a, b, c. \end{aligned} \tag{9}$$

Consequently, the three-phase symmetric model of this studied system can be pictured as shown in Fig. 5. Note that $G_c(s)$ in the block is given by (2).

III. Analyses of VSC Terminal Voltage Dynamics in the Current Control Time-Scale

This section elaborates on the mechanism for terminal voltage change and our research strategy for this topic. Based on the underlying mechanism, we propose using a corresponding small-signal model for analyzing the terminal voltage dynamics. The benefit of such a model is that it can distinguishes between the different influences of each part on the terminal voltage.

A. Mechanism of Terminal Voltage Change

The VSC can be seen as a kind of energy conversion device that transforms the energy from the DC link to the grid. The primary aim of a VSC control scheme is to control the switching mode of all insulated-gate bipolar transistors (IGBTs) to form a converter voltage vector with a controlled amplitude and phase angle, where the differences between the converter voltage vector and the grid voltage vector cause the active and reactive power flows. Thus, the studied system can be simplified as shown in Fig. 6, where a controllable VSC attaches to the grid voltage source via a LC filter and the grid impendence. Such a

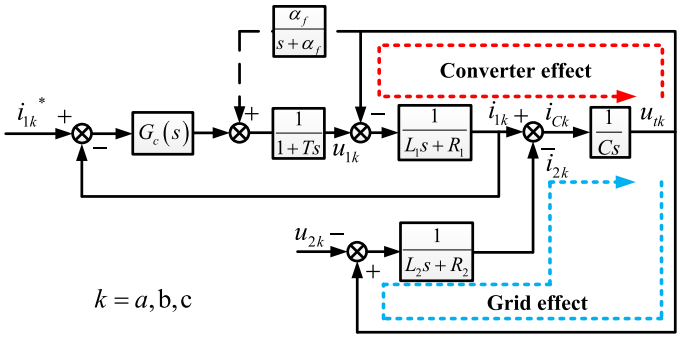

Fig. 6. Simplified schematic diagram of the studied single-phase representation system.

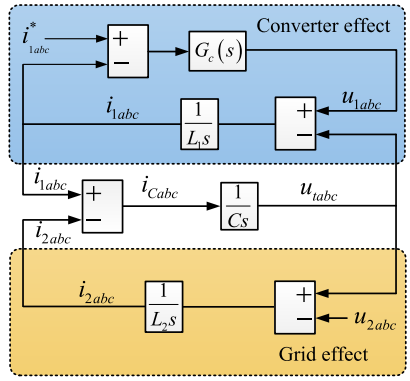

Fig. 7. Block diagram of terminal voltage change mechanism.

typical model is useful for explaining some basic concepts concerning the influencing factors and mechanisms behind terminal voltage dynamics.

In this simplified model, the VSC terminal voltage u_t interacts with the converter voltage u_1 and grid voltage u_2 to create converter current i_1 and grid current i_2, respectively. For the capacitor of the LC filter, the converter current i_1 is the input current and the grid current i_2 is the output current. The difference between the capacitor input current i_1, from the VSC side, and the output current i_2, flowing to the grid, is the current i_C, which flows through the capacitor.

$$i_C = i_1 - i_2. \tag{10}$$

Because of the nature of capacitance, there is also a clear mathematical relationship between the voltage u_t across the capacitor and the current i_C, written as

$$C\frac{d}{dt}\begin{bmatrix} u_{ta} \\ u_{tb} \\ u_{tc} \end{bmatrix} = \begin{bmatrix} i_{Ca} \\ i_{Cb} \\ i_{Cc} \end{bmatrix}. \tag{11}$$

Fig. 7 illustrates the VSC terminal voltage formation mechanism. From the figure, it is evident that both the converter and the grid can affect terminal voltage dynamics. The voltage across the capacitor, namely the terminal voltage, cannot change suddenly. On the converter side, the error between the current reference and the measured value is imported into the current controller to form the converter voltage. At this point, the converter current through the impedance of the filter inductor is created by the difference between the converter voltage u_1 and the VSC terminal voltage u_t. The grid side current i_2 through the impedance of the grid inductor is created by the difference between the VSC terminal voltage and the grid voltage. As mentioned above, the difference between the converter current and grid current determines the voltage across the filter capacitor as well as the VSC terminal voltage.

At least two important conclusions about this terminal voltage dynamics stability mechanism in the current control time-scale can be made, viz., (a) the VSC terminal voltage is affected by both the converter side and the grid side, and (b) determining how the converter current and grid current behave in a dynamic process is the core problem that must be investigated to analyze VSC terminal voltage dynamics.

Several factors have been found to have a significant influence on terminal voltage dynamics in the current control time-scale. This paper will focus on the effects of the VSC current controller, the VFF scheme and the strength of the AC grid on terminal voltage dynamics in following sections.

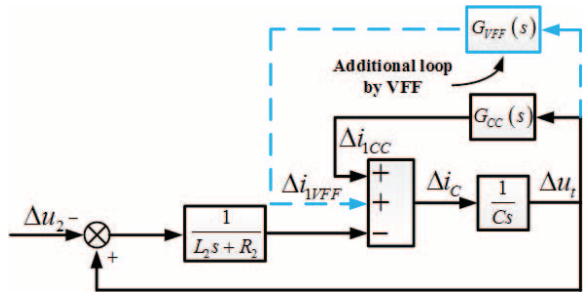

Fig. 8. Simplified schematic for analyzing the effects of different parts of the system on the terminal voltage.

B. Small-Signal Modelling of a VSC System

As mentioned above, the voltage dynamics of the current control time-scale have some unique characteristics. Thus, it is first necessary to propose a valid model that considers the dynamic characteristics of the system in the current control time-scale.

In order to analyze the stability of the terminal voltage dynamics, the mathematical model should be linearized. In the current control time-scale, the current references can be regarded as constants, with $\Delta i_1^* = 0$. In a VSC without VFF, the following set of equations describe the voltage and current conditions for small perturbations.

$$\begin{cases} \Delta u_1 = -\left(K_p + \frac{K_i s}{s^2+\omega_0^2}\right)\left(\frac{1}{1+Ts}\right)\Delta i_1 \\ \Delta i_1 = \frac{1}{L_1 s + R_1}\left(\Delta u_1 - \Delta u_t\right) \\ \Delta i_2 = \frac{1}{L_2 s + R_2}\left(\Delta u_t - \Delta u_2\right) \\ \Delta i_C = Cs\Delta u_t = \Delta i_1 - \Delta i_2 \end{cases} \tag{12}$$

By using the simplified method described by the control block diagram in Fig. 7, we can arrive at the simplified linearized model illustrated in Fig. 8. In the figure, $G_{CC}(s)$ and $G_{VFF}(s)$ represent the transfer functions of the current control and the VFF, respectively.

It is obvious from the figure that $G_{CC}(s)$ and $G_{VFF}(s)$ represent the influence of the converter. Furthermore, the input current Δi_1 consists of two aspects, described by

$$\Delta i_1 = \Delta i_{1CC} + \Delta i_{1VFF}. \tag{13}$$

This model sets grid voltage u_2 to be the input perturbation. In order to highlight every section's effects on the terminal voltage, the effects of the current control and the VFF are clearly indicated in the figure by using with two loops over the capacitor voltage equation.

By using this small-signal model, the effects of current control, VFF and AC grid strength on the terminal voltage dynamics stability can be analyzed from the perspective of terminal voltage damping in the following sections.

IV. Stability Analysis

A. Effects of Current Control on Terminal Voltage Dynamics

As shown in Fig. 8, current control is the primary component of VSC control in the current control time-scale. The effects of current control on terminal voltage dynamics can be investigated through the amplitude-frequency and phase-frequency characteristics of its transfer function.

That transfer function for the current control is derived from (12) to become

$$\Delta i_{1CC} = -\underbrace{\frac{1+Ts}{(L_1 s + R_1)(1+Ts) + G_c(s)}}_{G_{CC}(s)} \Delta u_t \qquad (14)$$

where $G_c(s)$ is the current controller transfer function as defined by (2).

For this frequency domain analysis, the current control bandwidth was set to a value of $f_b = 200$ Hz (in the strong grid condition), while the remaining practical parameters can be found in Appendix A. It is worth mentioning that the bandwidth of current control described in this paper is defined in the same positive sequence dq rotating reference frame in which the PI controller is implemented.

Bode plots of $G_{CC}(s)$ are given as Fig. 9. In the current control time-scale, the phase-frequency response is between 180° and 90°. This means that the VSC current control can provide significant positive damping in the frequency region of the current control time-scale. Moreover, when the bandwidth is shifted from 200 Hz to 165 Hz or 135 Hz, the amplitude-frequency characteristics in these different controller bandwidths are almost identical, while the phase-frequency response decreases closer to 90° as the bandwidth decreases. That means that the damping provided by the current control decreases as the bandwidth decreases. The phasor diagram provides a graphical way to investigate the effects of the current controller on terminal voltage dynamics. Using the amplitude and phase frequency response of $G_{CC}(s)$ shown in Fig. 9, the phasor of the current component caused by the current control with different bandwidths at 80 Hz is illustrated in Fig. 10. It is obvious from the figure that the phasor of the current controller effect is in the positive damping region, and that the damping decreases as the bandwidth decreases. The positive damping region indicates that the current decreases when the terminal voltage increases, and the change of current is beneficial for terminal voltage dynamics stability. On the other hand, the negative damping region indicates that the current increases when the terminal voltage increases. As a result, any change in current adversely affects stability of the terminal voltage.

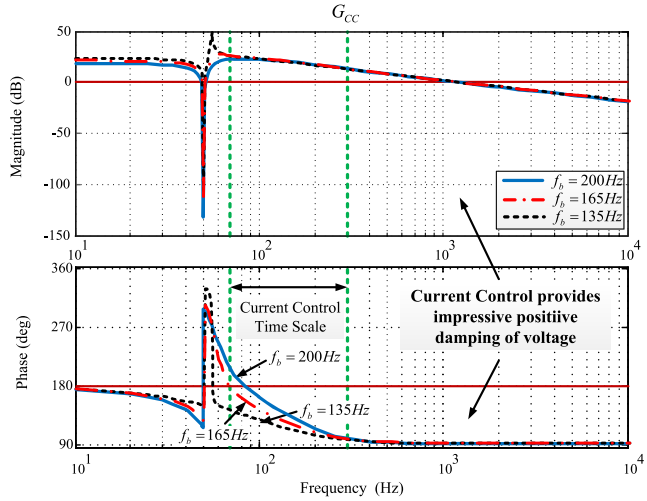

Fig. 9. Bode plots of G_{CC} with different control bandwidths.

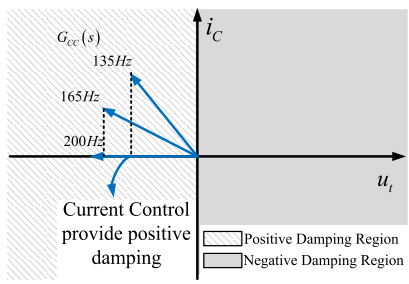

Fig. 10. Phasor diagram of $G_{CC}(s)$ at 80 Hz (in the current control time-scale).

B. Effect of Using VFF on Terminal Voltage Dynamics

The VFF technique is commonly used for improving the anti-disturbance nature of the converter current in a VSC current control scheme. This type of settlement guarantees a relatively steady converter current output but ignores stability of the terminal voltage. The current of a converter with an ideal VFF does not respond to grid disturbances. Thus, it is undoubtedly a good idea to improve the anti-disturbance quality of the converter current but only if the VSC connects to a stiff grid or if there is other equipment that can ensure the stability of the terminal voltage dynamics.

However, when the converter is attached to a weak grid, the VSC terminal voltage will be more affected by the converter itself. In such a system, a control strategy that does not sure terminal voltage dynamics stability will cause the terminal voltage to severely fluctuate or even become unstable. To put it succinctly, a converter control strategy that keeps a VSC output stable does not necessarily promote whole system stability. In fact, the objectives of improving stability of an individual equipment versus maintaining the stability of the whole system can be contradictory. Note that if the system becomes unstable, a single VSC will not survive by itself. Consequently, the impact of VFF on VSC terminal voltage must be seriously considered in the current control time-scale.

1) VFF With Different Filter Bandwidths: Given a VFF loop which is a feedback from u_t, the loop includes the current controller $G_c(s)$, the delay part of the VSC $G_d(s)$, VFF low-pass

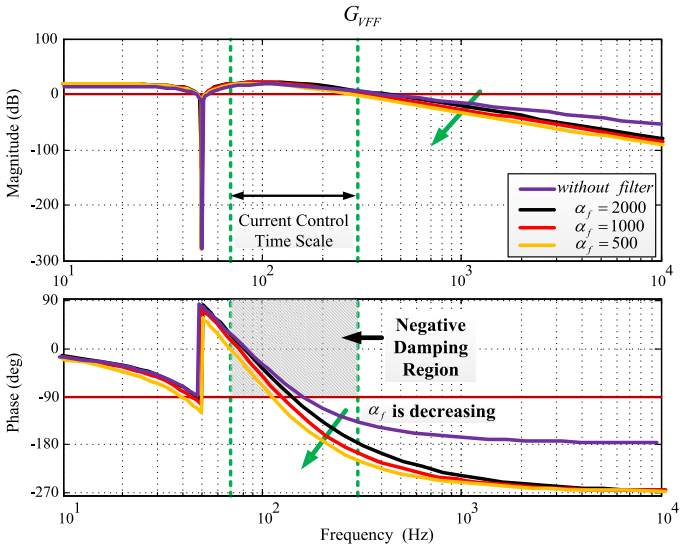

Fig. 11. Bode plots of $G_{VFF}(s)$ with different filter bandwidths.

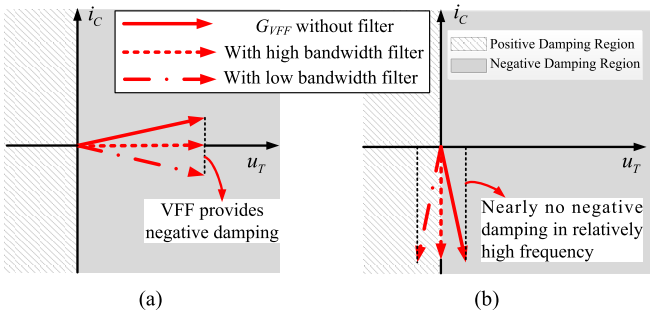

Fig. 12. Phasor diagram of $G_{VFF}(s)$ at different frequencies: (a) phasor diagram of $G_{VFF}(s)$ at 80 Hz, and (b) phasor diagram of $G_{VFF}(s)$ at 150 Hz.

filter $G_l(s)$ (used to improve disturbance rejection), and the VSC filter inductance. The transfer function from the VSC terminal voltage u_t to i_{1VFF} is

$$\Delta i_{1VFF} = \underbrace{\underbrace{\frac{\alpha_f}{s+\alpha_f}}_{G_l(s)} \frac{1}{(L_1 s + R_1)(1+Ts) + G_C(s)}}_{G_{VFF}(s)} \Delta u_t \tag{15}$$

where $G_l(s)$ is an approximated transfer function describing the low-pass filter.

The relationship between Δi_1 and Δu_t determines the effects of the two feedback loops. Fig. 11 shows the bode plot of $G_{VFF}(s)$ for different filter bandwidths. Note that VFF without a filter means that α_f is infinite. In the region of the current control time-scale frequency around 80 Hz, the phase lag of $G_{VFF}(s)$ is between $-90°$ and $90°$, which represents the negative damping region. Therefore, the VFF provides a negative damping component for a given frequency band of the current control time-scale. In a higher frequency range around 150 Hz, the phase lag of $G_{VFF}(s)$ is approximately $-90°$, which indicates that the VFF is providing little negative damping. As the filter bandwidth decreases, the frequency range of the VFF providing the most serious negative damping also decreases. Consequently, given other identical conditions, the oscillation frequency decreases along with the filter bandwidth.

The phasors of the current component caused by the VFF, due to the Bode characteristics of $G_{VFF}(s)$ with different filter bandwidths under different frequencies, are drawn in Fig. 12(a) and (b) at 80 Hz and 150 Hz, respectively. Note that the phasor of the VFF effect is in the negative damping region around 80 Hz, while the projection of the phasor on the horizontal axis is nearly zero at higher frequencies. Thus, the damping status of $G_{VFF}(s)$ is clearly revealed in the figure.

We can derive the transfer functions (u_t/u_2) of converter without and with VFF ($G_{ol}(s)$ and $H_{ol}(s)$, respectively) for the whole system. The open-loop transfer functions (u_t/u_2) of the two schemes are given by

$$G_{ol}(s) = \frac{1}{(L_2 s + R_2)(Cs - G_{CC})} \tag{16}$$

without VFF, and

$$H_{ol}(s) = \frac{1}{(L_2 s + R_2)(Cs - G_{CC}(s) - G_{VFF}(s))} \tag{17}$$

with VFF.

2) VFF With Auxiliary Active Damping: It is possible to alter the effects of VFF by changing the characteristics of $G_{VFF}(s)$. In order to improve self-stability, [20] proposed an active damping method, which used a lead-lag element applied to the VFF. The transfer function of VFF with active damping $G_{VFF}(s)$ can be written as

$$G_{VFF}(s) = \underbrace{K_{ll}\frac{1+T_n s}{1+T_d s}}_{Activedamping} \underbrace{\frac{\alpha_f}{s+\alpha_f}}_{G_l(s)} \cdot \frac{1}{(L_1 s + R_1)(1+Ts) + G_C(s)}. \tag{18}$$

By using this method, an active damping element is added in the VFF for providing damping in the current control time-scale. A comparison of Bode plots of the VFF with and without active damping is shown in Fig. 13. It is worth noting that the active damping method changes the VFF transfer function characteristics, and evidently provides positive damping in the current control time-scale.

3) Stability Analysis of Different VSC Control Schemes: As seen in Fig. 8, the combination of positive damping provided by current control and the negative damping provided by VFF describes the entire converter effect on terminal voltage dynamics. Thus, the dynamics of the terminal voltage are determined by the characteristics of both the converter and the grid.

Fig. 14 shows the open-loop Bode plots (u_t/u_2) of the complete system with different converter control schemes. Given identical grid conditions (an extremely weak grid with impedance $L_2 = 0.45$ mH), the three different control schemes produce different stability margins, with the terminal voltage becoming unstable when VFF is used in the VSC. It is clear that the phase margin of a control scheme without VFF is much larger than for a control scheme with VFF. Moreover, the terminal voltage is stable when the VSC uses VFF with an active damping element. From these above stability analysis, we can see that VFF provides negative damping to the terminal voltage

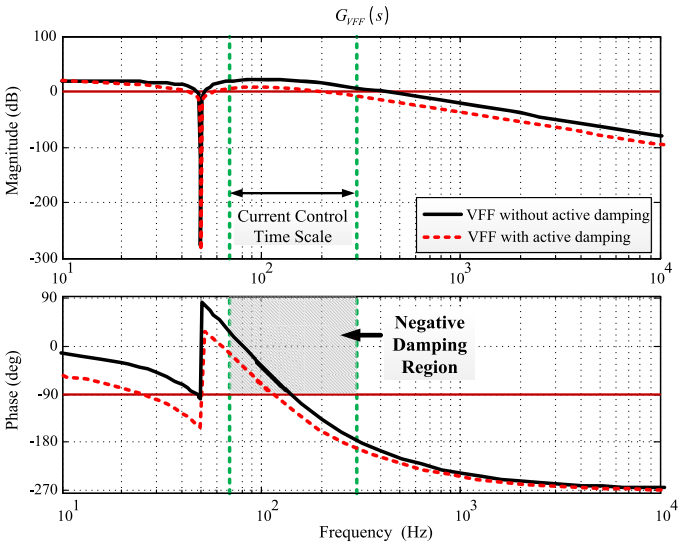

Fig. 13. Bode plots of $G_{VVF}(s)$ with and without active damping.

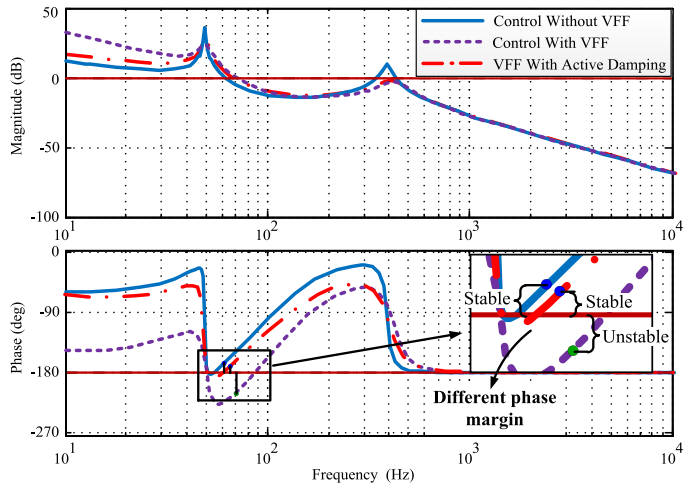

Fig. 14. Bode plots of VSC with and without a VFF open-loop transfer function (u_t/u_2).

in a specific frequency range belonging to the current control time-scale, which deteriorates terminal voltage dynamics stability. However, the active damping method proposed by [20] can provide damping to the VSC, which stabilizes the terminal voltage.

C. *Effect of Grid Strength on Terminal Voltage Dynamics*

Another critical factor of the voltage oscillatory instability problem is the strength of the AC grid to which the power electronics are integrated. In the studied system shown in Fig. 7, both sides of the filter capacitor have damping effects on the VSC terminal voltage. On the grid side, the resistance in the grid acts as a damping for the VSC terminal voltage. On the converter side, the current controller will provide positive damping without VFF or negative damping over some frequency range with VFF. Moreover, the strength of the grid determines the proportion of impact the converter and grid have on the VSC terminal voltage.

Different from analysis in the stationary reference frame, the linearized model is used to analyze the effect of grid strength in the synchronous reference frame, and includes the decoupling terms of the current controllers. Some studies have looked at the small-signal modeling of grid-connected VSCs [29]–[32], such as wind turbine converters and VSC-HVDC systems. This method, which is used to model the subject investigated by this paper, is quite mature. Consequently, the specific process for developing this model is not undertaken here, and can be found in the references noted above. Moreover, it is worth noting that this model does consider a phase-locked loop (PLL). Fig. 15 shows the eigenvalue distribution of the VSC with and without VFF for a grid impedance varying from 0.09 mH to 0.45 mH. For the converter control without VFF, both converter and grid affect the VSC terminal voltage. Therefore, the terminal voltage remains stable when the VSC integrates to an extremely weak grid (i.e., a grid impendence of more than 0.45 mH). The change in eigenvalues as the grid becomes weaker is shown in Fig. 15(a).

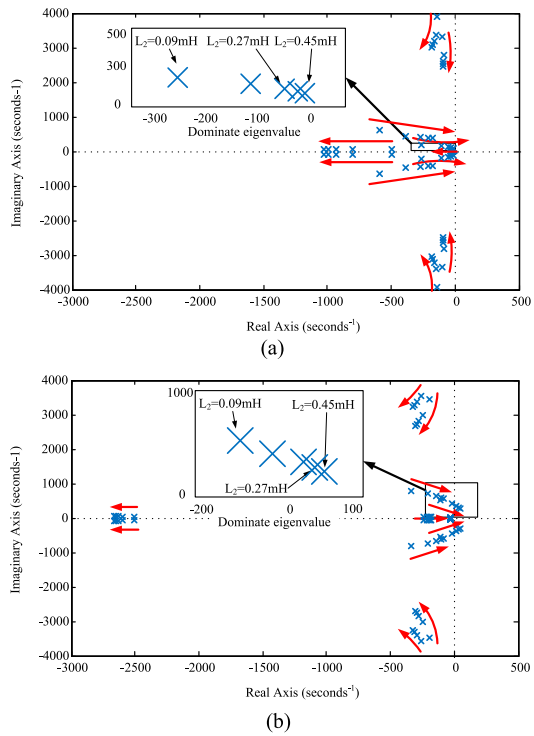

Fig. 15. Variation in system eigenvalues with grid strength L_2 varying from 0.09 mH to 0.45 mH. (a) current control without VFF, and (b) current control with VFF.

On the other hand, when the converter control involves VFF, the terminal voltage dynamics stability is deteriorated due to the negative damping providing by the VFF. In this scenario, a weaker grid means that the converter side has more impact on terminal voltage dynamics stability, as does the negative effect provided by the VFF. Therefore, the terminal voltage becomes unstable as the grid impendence increases to 0.45 mH. The change in system eigenvalues for this system is illustrated in Fig. 15(b). Table I shows the dominant eigenvalues of the VSC with and without VFF for different grid strengths.

TABLE I
DOMINANT EIGENVALUES OF VSC WITH AND WITHOUT VFF FOR VARIOUS GRID IMPENDENCE VALUES

Grid impendence	Dominant eigenvalues	
	VSC without VFF	VSC with VFF
0.09mH	-262± j206	-110± j527
0.27mH	-54.7± j143	17.4± j366 (unstable)
0.45mH	-12.7± j101	46± j284 (unstable)

TABLE II
SENSITIVITY ANALYSIS OF THE DOMINANT EIGENVALUES OF A VSC WITH VFF UNDER $L_2 = 0.21$ mH

Dominant eigenvalue	Parameters	Eigenvalue sensitivity
-37.1± 462.3i	K_p	-265.9
	K_i	1.04
	L_2	431.25

D. Eigenvalue Sensitivity and Marginal Values of the Critical Parameters of the System

The above subsections have analyzed the three main factors influencing terminal voltage dynamics stability in the current control time-scale. However, there are several system parameters that can also influence stability to a different extent. Thus, it is necessary to examine the sensitivity of these parameters, a process that can significantly guide the design of converter parameters.

The sensitivity of a dominant eigenvalue λ_i to specified parameters K_j can be derived from

$$\frac{\partial \lambda_i}{\partial K_j} = \frac{\boldsymbol{N}_i^T \frac{\partial \boldsymbol{A}}{\partial K_j} \boldsymbol{M}_i}{\boldsymbol{N}_i^T \boldsymbol{M}_i} \tag{19}$$

where $\boldsymbol{N}_i$ and $\boldsymbol{M}_i$ represent the left and right eigenvectors to λ_i respectively. The $\boldsymbol{A}$ matrix is the state matrix of the whole system after linearization, which is in the dq synchronous reference frame. The specified expression of the $\boldsymbol{A}$ matrix is shown in Appendix. It is necessary to note that, for simplicity, the $\boldsymbol{A}$ matrix does not include the PLL dynamics.

Compared with the imaginary part of the eigenvalue, the real part of the eigenvalue sensitivity is more important as a system characteristic. Thus, the results of a sensitivity analysis for the real part of the eigenvalue are shown in Table II.

From the analysis, we found that the K_p and K_i of the VSC need to be properly designed, and L_2 varies according to different system conditions, while the remaining parameters of the VSC are fixed. Thus, Table II focuses on the eigenvalue sensitivities of K_p, K_i and L_2. Note that the three critical parameters have different sensitivities. K_p and L_2 are the most critical parameters for the dominant eigenvalue. Moreover, the sensitivities of K_p and L_2 are negative and positive, that is the system become stable as K_p increases or L_2 decreases.

Another useful way to quantify this phenomenon is to plot the allowed range of the minimum current control parameter K_p against grid strength, with the aim of maintaining stability, as shown in Fig. 16. From this guidance, we can see that K_p should be designed to be higher as the integrated grid gets weaker.

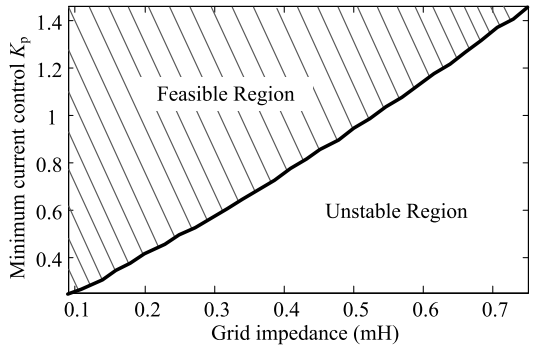

Fig. 16. Grid strength versus minimum current control K_p for a stable terminal voltage.

V. SIMULATION RESULTS

The configuration and control system of a VSC integrated with a grid, as proposed in Figs. 3 and 4, was tested to verify the effects of the current controller, VFF and grid strength on terminal voltage dynamics. Simulations were carried out to validate the analyses described in the previous section.

Fig. 17(a) shows the terminal voltage responses under a sudden grid voltage amplitude change (a 0.05 pu grid voltage disturbance) using different current controller bandwidths (without VFF). The simulation was conducted using a grid impendence value of $L_2 = 0.21$ mH (i.e., a relatively weak grid). The figure illustrates that the damping provided by the current control decreases as the bandwidth decreases. Fig. 17(b) describes VSC integrated into a relatively stiff grid ($L_2 = 0.09$ mH) with different VFF filter bandwidths, while Fig. 17(c) and (d) verify the effects of VFF and grid strength on terminal voltage dynamics stability. In a relatively stiff grid ($L_2 = 0.09$ mH), the terminal voltage is stable after a grid side disturbance, and the damping ratio of VSC controller without VFF is higher than with VFF. In a relatively weak grid ($L_2 = 0.21$ mH), the terminal voltage becomes unstable when the VSC controller adopts a VFF technique. Accordingly, the terminal voltage of a VSC that does not adopt VFF, remains stable when using the active damping proposed in [20]. Fig. 17(d) shows these simulation results, validating our conclusion that VFF causes negative damping to the terminal voltage, and that this negative effect is aggravated as a grid weakens.

VI. DISCUSSION

The parameters in the analyzed system all have their physical meanings. Understanding these physical meanings is useful for analyzing VSC terminal voltage dynamics stability.

The ratio of the LC filter inductance to grid impedance indicates which of the two voltage vectors—converter side or grid side have more an effect on the VSC terminal voltage. Generally speaking, the inductance of the LC filter is fixed by filter design while the equivalent impedance of the grid is alterable as the grid state changes. Therefore, the VSC terminal voltage is more affected by the converter voltage as the grid becomes weaker.

In addition, the capacitance of the LC filter is the inertia of the VSC terminal voltage. If the capacitor is large enough, the

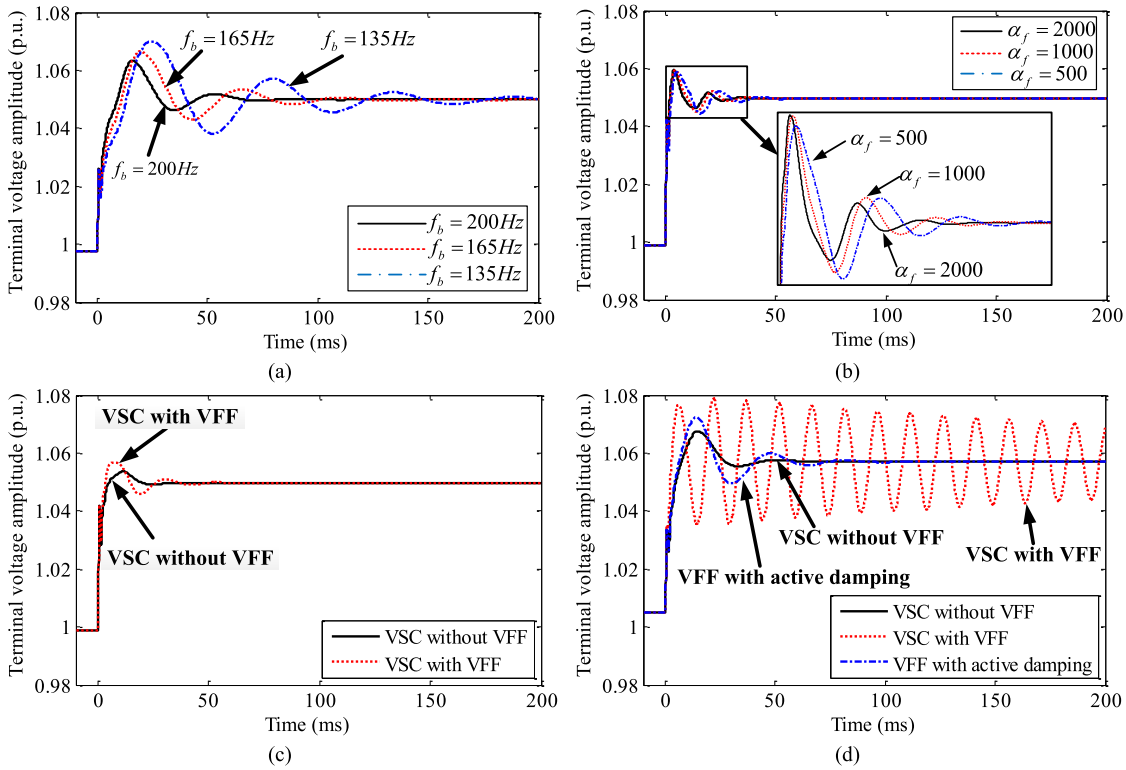

Fig. 17. Terminal voltage response for a sudden change in grid voltage amplitude: (a) terminal voltage response with different CC bandwidths ($L_2 = 0.21$ mH and without VFF); (b) terminal voltage response with different VFF filter bandwidths ($L_2 = 0.09$ mH); (c) terminal voltage responses with or without VFF in a relatively stiff grid ($L_2 = 0.09$ mH); and (d) terminal voltage response of the VSC with and without VFF and with VFF with active damping in a relatively weak grid ($L_2 = 0.21$ mH).

VSC terminal voltage amplitude is not so easy to change when the input and output currents change, whereas the amplitude changes a lot with a small capacitance.

Actually, a PLL also influences terminal voltage dynamics in the current control time-scale, such that the damping of the system is overestimated when ignoring the PLL. However, the PLL complicates modeling and analysis, and also has a relatively small effect on terminal voltage dynamics in comparison to the other factors analyzed in Section IV. Thus, there is no specific analysis of the PLL's influence in this paper due to space limit, but is a concept that will be further analyzed in future work.

VII. Conclusion

An extended classification method of transient time-scale for describing the voltage dynamics problem was proposed in this paper, which contains terminal voltage control and current control time-scale. In current control time-scale, the issues of voltage dynamics can also be divided as amplitude and phase stability problem, while this paper analyzes terminal voltage dynamics stability as a whole. Several analyses can be taken from terminal voltage amplitude stability and phase stability in the future work. The terminal voltage dynamics stability phenomenon and factors influencing stability in a VSC's current control time-scale have been sufficiently explored. Furthermore, we elaborated on the mechanisms behind the changes in a VSC's terminal voltage caused by a current-controlled VSC connected to a grid with a LC filter. The effects of VSC current control with and without VFF and with different grid strengths on terminal voltage dynamics stability were presented through theoretical analysis, then validated by simulations. The following are some conclusions resulting from this analysis.

- The VSC terminal voltage is determined by the difference between the converter current and the grid current. Thus, both the converter side and the grid side of the LC filter capacitor can affect the terminal voltage.
- VFF inserts an additional loop into the control that acts as a negative damping component for the terminal voltage, while the current control loop provides a positive damping component. Thus, VFF reduces stability of the terminal voltage especially in weak grids. However, proper active damping added to the VFF can improve this electrical damping characteristic.

TABLE III
Studied System Parameters

Grid voltage	U_1	690V
System capacity	S	2MW
Network	L_2, R_2	relatively stiff grid: 0.09mH, relatively weak grid: 0.21mH, extremely weak grid: 0.45mH 0.01Ω
LC filter	L_1, R_1	0.13mH, 0.005Ω
	C	1500μF
VSC current controller	K_p, K_i	K_p=0.5, K_i=100
Fund. Freq		50Hz
Switching Freq		2kHz
Sample time	T_s	0.5ms

$$\mathrm{A}=\begin{bmatrix} 0 & \omega_b & \frac{\omega_b}{C} & -\frac{\omega_b}{C} & 0 & 0 & 0 & 0 & 0 & 0 \\ -\omega_b & 0 & 0 & 0 & -\frac{\omega_b}{C} & \frac{\omega_b}{C} & 0 & 0 & 0 & 0 \\ -\frac{\omega_b}{L_1} & 0 & -R_1\frac{\omega_b}{L_1} & 0 & 0 & \omega_b & \frac{\omega_b}{L_1} & 0 & 0 & 0 \\ 0 & -\frac{\omega_b}{L_1} & -\omega_b & 0 & 0 & -R_1\frac{\omega_b}{L_1} & 0 & \frac{\omega_b}{L_1} & 0 & 0 \\ \frac{\omega_b}{L_2} & 0 & 0 & -R_2\frac{\omega_b}{L_2} & \omega_b & 0 & 0 & 0 & 0 & 0 \\ 0 & \frac{\omega_b}{L_2} & 0 & -\omega_b & -R_2\frac{\omega_b}{L_2} & 0 & 0 & 0 & 0 & 0 \\ 0 & 0 & -\frac{k_p}{T} & 0 & 0 & -\frac{L_1}{T} & -\frac{1}{T} & 0 & \frac{1}{T} & 0 \\ 0 & 0 & \frac{L_1}{T} & 0 & 0 & -\frac{k_p}{T} & 0 & -\frac{1}{T} & 0 & \frac{1}{T} \\ 0 & 0 & -k_i & 0 & 0 & 0 & 0 & 0 & 0 & 0 \\ 0 & 0 & 0 & 0 & 0 & -k_i & 0 & 0 & 0 & 0 \end{bmatrix} \tag{A.1}$$

$$\mathrm{A}=\begin{bmatrix} 0 & \omega_b & \frac{\omega_b}{C} & -\frac{\omega_b}{C} & 0 & 0 & 0 & 0 & 0 & 0 \\ -\omega_b & 0 & 0 & 0 & -\frac{\omega_b}{C} & \frac{\omega_b}{C} & 0 & 0 & 0 & 0 \\ -\frac{\omega_b}{L_1} & 0 & -R_1\frac{\omega_b}{L_1} & 0 & 0 & \omega_b & \frac{\omega_b}{L_1} & 0 & 0 & 0 \\ 0 & -\frac{\omega_b}{L_1} & -\omega_b & 0 & 0 & -R_1\frac{\omega_b}{L_1} & 0 & \frac{\omega_b}{L_1} & 0 & 0 \\ \frac{\omega_b}{L_2} & 0 & 0 & -R_2\frac{\omega_b}{L_2} & \omega_b & 0 & 0 & 0 & 0 & 0 \\ 0 & \frac{\omega_b}{L_2} & 0 & -\omega_b & -R_2\frac{\omega_b}{L_2} & 0 & 0 & 0 & 0 & 0 \\ \frac{1}{T} & 0 & -\frac{k_p}{T} & 0 & 0 & -\frac{L_1}{T} & -\frac{1}{T} & 0 & \frac{1}{T} & 0 \\ 0 & \frac{1}{T} & \frac{L_1}{T} & 0 & 0 & -\frac{k_p}{T} & 0 & -\frac{1}{T} & 0 & \frac{1}{T} \\ 0 & 0 & -k_i & 0 & 0 & 0 & 0 & 0 & 0 & 0 \\ 0 & 0 & 0 & 0 & 0 & -k_i & 0 & 0 & 0 & 0 \end{bmatrix} \tag{A.2}$$

$$\Delta\mathrm{X}=[\,\Delta u_{td}\quad \Delta u_{tq}\quad \Delta i_{1d}\quad \Delta i_{1q}\quad \Delta i_{2d}\quad \Delta i_{2q}\quad \Delta u_{1d}\quad \Delta u_{1q}\quad \Delta x_d\quad \Delta x_q\,]^T \tag{A.3}$$

- The critical parameters for terminal voltage dynamics stability are the current controller gain K_p and the transmission line inductance L_2 (representing the grid strength), both of which were demonstrated to have a high sensitivity to the dominant eigenvalues. The sensitivities of two parameters are calculated, positive and negative, and the guidance for current controller gain design to maintain system stability was given for different grid strengths.

APPENDIX

When the VSC control without VFF, the state matrix A of system is shown at the top of this page, and the state matrix A of the VSC using VFF technique and the state vector of system are (A.1)–(A.3) at the top of this page.

REFERENCES

[1] R. Piwko, N. Miller, J. Sanchez-Gasca, X. Yuan, R. Dai, and J. Lyons, "Integrating large wind farms into weak power grids with long transmission lines," in *Proc. IEEE Int. Power Electron. Motion Control Conf.*, 2006, vol. 3, pp. 1122–1128.

[2] J. Kabouris and F. D. Kanellos, "Impacts of large-scale wind penetration on designing and operation of electric power systems," *IEEE Trans. Sustain. Energy*, vol. 1, no. 2, pp. 107–114, Jul. 2010.

[3] H. Shun-Hsien, J. Schmall, J. Conto, J. Adams, Z. Yang, and C. Carter, "Voltage control challenges on weak grids with high penetration of wind generation: ERCOT experience," in *Proc. IEEE PES General Meeting*, San Diego, CA, USA, Jul. 22–26, 2011.

[4] P. Kundur *et al.*, "Definition and classification of power system stability IEEE/CIGRE joint task force on stability terms and definitions," *IEEE Trans. Power Syst.*, vol. 19, no. 3, pp. 1387–1401, Aug. 2004.

[5] T. Van Cutsem and C. D. Vournas, "Voltage stability analysis in transient and mid-term time scales," *IEEE Trans. Power Syst.*, vol. 11, no. 1, pp. 146–154, Feb. 1996.

[6] A. Kurita, H. Okubo, K. Oki, S. Agematsu, D. B. Klapper, N. W. Miller, W. W. Price, J. J. Sanchez-Gasca, K. A. Wirgau, and T. D. Younkins, "Multiple time-scale power system dynamic simulation," *IEEE Trans. Power Syst.*, vol. 8, no. 1, pp. 216–223, Feb. 1993.

[7] C. D. Vournas, P. W. Sauer, and M. A. Pai, "Time-scale decomposition in voltage stability analysis of power systems," in *Proc. 34th IEEE Conf. Decision and Control*, New Orleans, LA, USA, 1995, vol. 4, pp. 3459–3464.

[8] E. G. Cate, K. Hemmaplardh, J. W. Manke, and D. P. Gelopulos, "Time frame notion and time response of the models in transient, mid-term and long-term stability programs," *IEEE Power Eng. Rev.*, vol. PER-4, no. 1, p. 39, 1984.

[9] V. Ajjarapu and C. Christy, "The continuation powerflow: A tool for steady state voltage stability analysis," *IEEE Trans. Power Syst.*, vol. 7, no. 1, pp. 416–423, Feb. 1992.

[10] B. Gao, G. K. Morison, and P. Kundur, "Voltage stability evaluation using modal analysis," *IEEE Trans. Power Syst.*, vol. 7, no. 4, pp. 1529–1542, Nov. 1992.

[11] E. Vittal, M. O'Malley, and A. Keane, "A steady-state voltage stability analysis of power systems with high penetrations of wind," *IEEE Trans. Power Syst.*, vol. 25, no. 1, pp. 433–442, Feb. 2010.

[12] T. Midtsund, J. A. Suul, and T. Undeland, "Evaluation of current controller performance and stability for voltage source converters connected to a weak grid," in *Proc. IEEE Power India Conf.*, Kolkata, India, 2010, pp. 382–388.

[13] J. Martinez, P. C. Kjar, P. Rodriguez, and R. Teodorescu, "Comparison of two voltage control strategies for a wind power plant," in *Proc. IEEE Power & Energy Soc. Power Systems Conf.*, Phoenix, AZ, USA, Mar. 20–23, 2011.

[14] J. Martinez, P. C. Kjer, and R. Teodorescu, "DFIG turbine representation for small signal voltage control studies," in *Proc. 12th Int. Conf. Optimization Elect. Electron. Equipment*, May 20–22, 2010, pp. 31–40.

[15] J. Martinez and P. C. Kjaer, "Fast voltage control in wind power plants," in *Proc. IEEE PES General Meeting*, San Diego, CA, USA, Jul. 24–29, 2011.

[16] L. Huijuan, L. Fangxing, X. Yan, D. Rizy, and J. Kueck, "Adaptive voltage control with distributed energy resources: Algorithm, theoretical analysis, simulation, and field test verification," *IEEE Trans. Power Syst.*, vol. 25, no. 3, pp. 1638–1647, Aug. 2010.

[17] S. De Rijcke, H. Ergun, D. Van Hertem, and J. Driesen, "Grid impact of voltage control and reactive power support by wind turbines equipped with direct-drive synchronous machines," *IEEE Trans. Sustain. Energy*, vol. 3, no. 4, pp. 890–898, Oct. 2012.

[18] F. Blaabjerg, R. Teodorescu, M. Liserre, and A. V. Timbus, "Overview of control and grid synchronization for distributed power generation systems," *IEEE Trans. Ind. Electron.*, vol. 53, no. 5, pp. 1398–1409, Oct. 2006.

[19] L. Ma, A. Luna, J. Rocabert, R. Munoz, F. Corcoles, and P. Rodriguez, "Voltage feed-forward performance in stationary reference frame controllers for wind power applications," in *Proc. 2011 Int. Conf. IEEE Power Engineering, Energy and Electrical Drives (POWERENG)*, Malaga, Spain, 2011.
[20] V. Blasko and V. Kaura, "A novel control to actively damp resonance in input LC filter of a three-phase voltage source converter," *IEEE Trans. Ind. Appl.*, vol. 33, no. 2, pp. 542–550, Mar. 1997.
[21] T. Abeyasekera, C. M. Johnson, D. J. Atkinson, and M. Armstrong, "Suppression of line voltage related distortion in current controlled grid connected inverters," *IEEE Trans. Power Electron.*, vol. 20, no. 6, pp. 1393–1401, Nov. 2005.
[22] L. Harnefors, "Analysis of subsynchronous torsional interaction with power electronic converters," *IEEE Trans. Power Syst.*, vol. 22, no. 1, pp. 305–313, Feb. 2007.
[23] K. Clark, N. W. Miller, and J. J. Sanchez-Gasca, Modeling of GE Wind Turbine-Generators for Grid Studies, ver. 4.5, General Electric International, Inc., Apr. 2010.
[24] S. Li, T. A. Haskew, K. A. Williams, and R. P. Swatloski, "Control of DFIG wind turbine with direct-current vector control configuration," *IEEE Trans. Sustain. Energy*, vol. 3, no. 1, pp. 1–11, Jan. 2012.
[25] X. Yuan, W. Merk, H. Stemmler, and J. Allmeling, "Stationary-frame generalized integrators for current control of active power filters with zero steady-state error for current harmonics of concern under unbalanced and distorted operating conditions," *IEEE Trans. Ind. Appl.*, vol. 38, no. 2, pp. 523–532, Mar./Apr. 2002.
[26] D. N. Zmood, D. G. Holmes, and G. H. Bode, "Frequency domain analysis of three-phase linear current regulators," *IEEE Trans. Ind. Appl.*, vol. 37, no. 2, pp. 601–610, Mar./Apr. 2001.
[27] E. Twining and D. G. Holmes, "Grid current regulation of a three-phase voltage source inverter with an LCL input filter," *IEEE Trans. Power Electron.*, vol. 18, no. 3, pp. 888–895, May 2003.
[28] J. Holtz and N. Oikonomou, "Fast dynamic control of medium voltage drives operating at very low switching frequency—An overview," *IEEE Trans. Ind. Electron.*, vol. 55, no. 3, pp. 1005–1013, Mar. 2008.
[29] L. Zhang, "Modeling and control of VSC-HVDC links connected to weak AC systems," Ph.D. dissertation, Royal Inst. Technol., Stockholm, Sweden, 2010.
[30] F. Wu, X.-P. Zhang, and P. Ju, "Modeling and control of the wind turbine with the direct drive permanent magnet generator integrated to power grid," in *Proc. 3rd Int. Conf. Electric Utility Deregulation and Restructuring and Power Technologies*, 2008, pp. 57–60.
[31] M. Durrant, H. Werner, and K. Abbott, "Model of a VSC-HVDC terminal attached to a weak AC system," in *Proc. 2003 IEEE Conf. Control Applications, 2003 (CCA 2003*, 2003, vol. 1, pp. 178–182.
[32] Y. Huang, X. Yuan, J. Hu, and P. Zhou, "Modeling of VSC connected to weak grid for stability analysis of DC-link voltage control," *IEEE J. Emerg. Select. Topics Power Electron.*, to be published.

Mingquan Zhao (S'14) was born in Tianjin, China. He received the B.Eng. degree from the School of Electrical and Electronic Engineering, Huazhong University of Science and Technology (HUST), Wuhan, China, in July 2010. He is currently working toward the Ph.D. degree with the State Key Laboratory of Advanced Electromagnetic and Technology, School of Electrical and Electronic Engineering, Huazhong University of Science and Technology.

His current research interests include grid-integration of large-scale renewable energy generations, in particular on the voltage dynamics analysis and control of semiconducting power systems.

Xiaoming Yuan (S'97–M'99–SM'01) received the B.Eng. degree from Shandong University, China, the M.Eng. degree from Zhejiang University, China, and the Ph.D. degree from Federal University of Santa Catarina, Brazil, in 1986, 1993, and 1998 respectively, all in electrical engineering.

He was with Qilu Petrochemical Corporation, China, from 1986 to 1990, where he was involved in the commissioning and testing of relaying and automation devices in power systems, adjustable speed drives, and high-power UPS systems. From 1998 to 2001, he was a Project Engineer at the Swiss Federal Institute of Technology Zurich, Switzerland, where he worked on flexible-ac-transmission-systems (FACTS) and power quality. From 2001 to 2008, he was with GE GRC Shanghai as a Manager of the Low Power Electronics Laboratory. From 2008 to 2010, he was with GE GRC US as an Electrical Chief Engineer. His research field involves stability and control of power system with multi machines multi converters, control and grid-integration of renewable energy generations, and control of high voltage dc transmission systems.

Dr. Yuan is Distinguished Expert of National Thousand Talents Program of China, and Chief Scientist of National Basic Research Program of China (973 Program). He received the first prize paper award from the Industrial Power Converter Committee of the IEEE Industry Applications Society in 1999.

Jiabing Hu (S'05–M'10–SM'12) received the B. Eng. and Ph.D. degrees in College of Electrical Engineering, Zhejiang University, Hangzhou, China, in July 2004 and September 2009, respectively. From 2007 to 2008, he was funded by Chinese Scholarship Council (CSC) as a visiting scholar with the Department of Electronic and Electrical Engineering, University of Strathclyde, Glasgow, U.K.

From April 2010 to August 2011, he was a Post-Doctoral Research Associate with Sheffield Siemens Wind Power (S2WP) research center and the Department of Electronic and Electrical Engineering, University of Sheffield, Sheffield, U.K. Since September 2011, he has been a professor with State Key Laboratory of Advanced Electromagnetic Engineering and Technology, and School of Electrical and Electronic Engineering, Huazhong University of Science and Technology, Wuhan, China. His current research interests include grid-integration of large-scale renewables, modular multilevel converter (MMC) for HVDC applications, and transient analysis and control of semiconducting power systems. He is the author/coauthor of more than 70 peer-reviewed technical papers and one monograph "Control and Operation of Grid-Connected Doubly-Fed Induction Generators", and holds more than 20 issued/pending patents.

Dr. Hu received the 2015 Delta Young Scholar Award from Delta Environmental and Educational Foundation, the 2014 TOP TEN Excellent Young Staff Award from Huazhong University of Science and Technology, and is currently supported by the National Natural Science of China for Excellent Young Scholars and the Program for New Century Excellent Talents in University from Chinese Ministry of Education. He serves as Associate Editor of *IET Renewable Power Generation*, and Domestic Member of the Editorial Board for *Frontiers of Information Technology and Electronic Engineering* (FITEE) formerly known as *Journal of Zhejiang University-SCIENCE C*.

Yabing Yan (S'14) was born in Hunan, China. He received the B.Eng. degree from the College of Hydropower & Information Engineering, Huazhong University of Science & Technology (HUST), Wuhan, China, in July 2012. He is currently working toward the Ph.D. degree with the State Key Laboratory of Advanced Electromagnetic Engineering and Technology, School of Electrical and Electronic Engineering, Huazhong University of Science and Technology, Wuhan, China.

His current research interests include control and stability analysis of grid-connected voltage-sourced converter, in particular on the stability of current control loop.